Countercurrent gas liquid flow in a PWR hot leg during reflux condensation

MURASE Michio[1], MINAMI Noritoshi[2], NAGAE Takashi[2], and TOMIYAMA Akio[3]

1. Institute of Nuclear Safety System, Inc., 64 Sata, Mihama-cho, Mikata-gun, Fukui 919-1205, Japan (murase@inss.co.jp)

2. The Kansai Electric Power Company, Inc., 13 Yokota 8, Goichi, Mihama-cho, Mikata-gun, Fukui 919-1141, Japan (minami.noritoshi@c4.kepco.co.jp, nagae.takashi@a5.kepco.co.jp)

3. Department of Mechanical Engineering, Kobe University, Rokkodai-cho 1-1, Nada, Kobe, Hyogo 657-8501, Japan (tomiyama@mech.kobe-u.ac.jp)

Abstract: The loss-of-RHR (residual heat removal systems) during mid-loop operation is one of the relatively high-risk events in pressurized water reactors. In order to increase reliability of transient analyses, the code scaling, applicability, and uncertainty methodology has been applied to evaluate the loss-of-RHR event, and a PIRT (phenomena identification and ranking table) for the event was developed. Based on the PIRT, important thermal-hydraulic behaviors during a loss-of-RHR event have been evaluated, and major results are summarized in this report. Reflux condensation by a steam generator is expected to be one of substitute methods of RHR cooling. In that case, countercurrent gas-liquid flow in the hot leg, which consists of horizontal, elbow and inclined sections, affects the reactor cooling system pressure and coolant level in the core. In order to evaluate flow patterns and CCFL (countercurrent flow limitation) characteristics in the hot leg, therefore, air-water experiments using small-scale models were carried out, and numerical simulations were conducted using a two-fluid model in FLUENT6.3.26. The calculated flow patterns and CCFL characteristics agreed well with the data. Flow patterns in the hot leg, which were split by the CCFL curve, were stratified flow without CCFL and wavy mist flow under CCFL conditions.

Keyword: loss-of-RHR; reflux condensation; countercurrent flow; PWR hot leg

1 Introduction

Nuclear power plants are periodically shut down for plant maintenance and refueling. During a PWR (pressurized water reactor) plant outage, reactor core cooling is achieved by RHR (residual heat removal systems). For a certain period, the reactor coolant level is kept around the primary loop center in order to carry out operations like aeration, attachment or detachment of the steam generator (SG) nozzle dam. This operation mode is called mid-loop operation. In some plants, a loss-of-RHR event during mid-loop operation occurred [1-2], and probabilistic safety assessment studies under plant shutdown conditions showed that the loss-of-RHR during mid-loop operation is a relatively high risk event for PWR plants. Therefore, experiments using integral test facilities [3-6] and analyses of the event progression [7] were conducted in order to investigate thermal-hydraulic phenomena and effectiveness of mitigation methods.

A more reliable analysis method is desirable to enhance reliability of mitigation methods. Therefore, at the Institute of Nuclear Safety System, Inc. (INSS), a statistical thermal-hydraulic analysis method based on the CSAU (code scaling, applicability and uncertainty evaluation) methodology [8] has been applied to evaluate the loss-of-RHR event during mid-loop operation using the best estimate analysis code, RELAP5/MOD3. The PIRT (phenomena identification and ranking table) and a verification matrix, which are essential in the CSAU methodology, were developed and RELAP5 void models, which are related to one of the important phenomena identified in the PIRT, were verified [9]. Based on the PIRT, important thermal-hydraulic behaviors during a loss-of-RHR event have been evaluated and major results are summarized in this report.

As a typical example of the important thermal-hydraulic behaviors during a loss-of-RHR event, details of countercurrent gas liquid flow in the PWR hot leg are also discussed.

Received date: August 8, 2010

2 Thermal-hydraulics during reflux condensation

2.1 Loss-of-RHR event and reflux condensation

The PIRT and verification matrix were developed for two representative scenarios of the loss-of-RHR event. One is an event with no openings in the RCS (reactor cooling system) and one of its mitigation methods is reflux condensation by one or two SGs. The other is an event with openings at the top of the pressurizer due to removal of safety valves. In this scenario SGs are isolated by nozzle plates and one of the mitigation methods is gravity injection from the RWST (refueling water storage tank) by manual operation. This scenario is called a gravity injection event. Success criteria for both scenarios are no core uncovery and no challenge to RCS boundary integrity. Hence, safety parameters evaluated are the reactor vessel (RV) water level and RCS pressure. The important technical issues in thermal hydraulics are mainly related to the reflux condensation and there are not many specific issues for the gravity injection event.

A schematic description of the reflux condensation in the RCS after core boiling is shown in Fig. 1. After the loss-of-RHR, core coolant temperature rises and eventually boiling occurs. Steam generation in the core swells the mixture level in the RV and RCS pressure gradually increases. Steam flows into the RCS air space and eventually flows into the cooling SG with air. Some water in the RV and hot leg may also flow up to the cooling SG in the steam flow. Steam flow into the cooling SG compresses the air and the steam is condensed due to contact with the SG tubes. Condensed water flows back to the RV through the hot leg. Countercurrent steam-water flow occurs in the hot leg and SG tubes. Air accumulation in the cooling SG tubes gradually increases as steam flow continues. Accumulation of air and water in the cooling SG decreases heat transfer in the SG and RCS pressure increases. RCS pressure depends on how much non-condensable gas and water accumulates in the cooling SG tubes.

2.2 Important thermal-hydraulic phenomena

Table 1 lists the technical issues for important thermal hydraulic phenomena during reflux condensation.

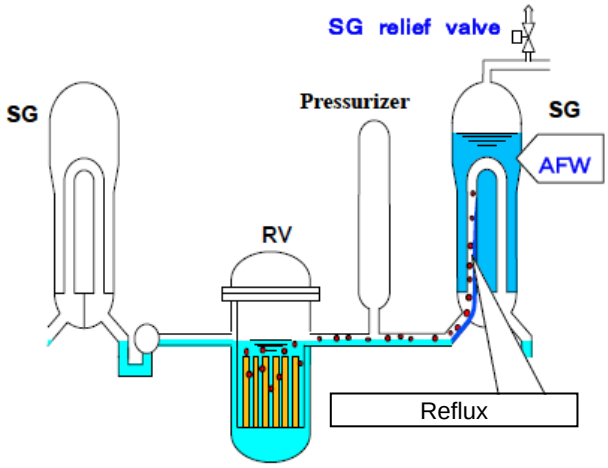

Fig.1 Schematic description of reflux condensation.

Table 1 Technical issues for important thermal-hydraulic phenomena during reflux condensation

Important phenomena	Technical issues
(1) Core and upper plenum: expansion of two-phase mixture	Lack of void data in a core under low pressure conditions
(2) Hot leg: flow patterns and CCFL characteristics	Lack of flow pattern data in elbow and inclined pipe
(3) SG tubes: condensation heat transfer in the presence of non-condensable gas	Lack of validation of condensation heat transfer correlations
(4) SG tubes: condensation heat transfer under low void fractions	Lack of condensation heat transfer data
(5) Pressurizer surge line: CCFL characteristics	Lack of CCFL data
(6) Pressurizer: discharge of non-condensable gas to hot leg	Lack of reliable information

(1) After the loss-of-RHR, coolant temperature increases and boiling initiates in the reactor core. Due to steam generation in the core, the mixture level of saturated steam and water increases in the RV, and coolant in the RV flows into the hot leg, SG and pressurizer. The behavior affects distribution of coolant and RCS pressure. Therefore, accurate evaluation of void fractions in the RV is important. However, void fraction data in the reactor core under low pressure and stagnant liquid conditions are quite limited. Then, void fraction measurements in rod bundles were conducted using an air-water system at Kobe University [10]. These results are discussed in section 2.3.

(2) After boiling in the reactor core, steam and water form countercurrent flow in the hot leg. Under these conditions, flow patterns and CCFL (countercurrent

flow limitation) characteristics in the hot leg affect the RCS pressure and the mixture level in the RV. Many CCFL tests have been conducted, but flow pattern maps in the hot leg under countercurrent flow conditions have not been reported. Therefore, air-water tests were carried out using a 1/5-scale model with a rectangular cross section [11] and a 1/15-scale model with a circular cross section [12] at Kobe University, and numerical simulations for the tests were conducted using a thermal-hydraulic analysis code FLUENT [13-14]. The results are shown in section 3 in detail.

(3) During mid-loop operation, space over the water surface in the RCS is filled with air (*i.e.* non-condensable gas). Therefore, a mixture of steam and air flows into the SG tubes, and air accumulates in the tubes due to steam condensation. Condensation heat transfer coefficients in the presence of non-condensable gas affect the RCS pressure. Many experiments on condensation of steam non-condensable gas mixture have been conducted. However, most of them are measurements of temperature distributions, and measurements of condensation heat transfer coefficients are few. Therefore, condensation heat transfer coefficients were measured at Purdue University and heat transfer correlations were derived [15]. Then SG reflux condensation behavior was calculated for the BETHSY experiments [4] using RELAP5/MOD3 with the derived correlations [16-17]. The results are discussed in the section 2.4.

(4) Due to expansion of the steam-water mixture, the mixture may reach a certain level in the SG tubes in a short time. Condensation heat transfer with low void fractions under the condition of mixture level formation has not been reported. The effects of the condensation heat transfer on the RCS pressure may not be significant because the mixture level in the SG tubes may not be high and the period of the mixture level formation may be short. Therefore, the effects will be evaluated in a future work.

(5) CCFL characteristics in the pressurizer surge line affect coolant accumulation in the pressurizer and water level in the RV. However, CCFL data in the surge line, which consists of an inclined pipe with small inclination angle, elbows and a vertical pipe, are quite limited. Therefore, air-water tests have been carried out at Kobe University [18]. The results are discussed in section 2.5.

(6) Some experimental and numerical studies indicated that air in the RV and RCS loop moves and accumulates in the SG, but the probability of movement of air in the pressurizer to the SG is uncertain. Steam and air behavior in the pressurizer during reflux condensation was, therefore, calculated numerically using FLUENT and the possibility of movement of air to the hot leg was investigated [19]. For a calculation domain, the pressurizer of ROSA-IV/LSTF [3] was employed: experimental data on the loss-of-RHR event during the mid-loop operation are available for this pressurizer. The calculated results indicated that the possibility of movement of air to the hot leg is low.

2.3 Void fractions in a core under stagnant liquid conditions

The correlation of void fractions proposed by Kataoka and Ishii [20] can be applied to wide ranges of diameters and fluid properties under stagnant liquid conditions, but its application is limited to circular tubes and vessels, because void fractions in a rod bundle differ from those in circular tubes due to the natural circulation caused locally between sub-channels. Therefore, void fractions under stagnant liquid conditions were measured in rod bundles simulating PWR and BWR (boiling water reactor) fuel assemblies using an air-water system at Kobe University [10].

Figure 2 shows the horizontal cross section of the rod bundle simulating a part of a PWR fuel assembly. The rod diameter and the rod pitch are 10 and 12.3 **mm**, respectively. The hydraulic diameter of the test section is 9.0 **mm**. Air was supplied from the compressor and injected into stagnant water through the diffuser plate in the lower tank. The diffuser plate was made of a porous medium and bubbles were injected from the plate. Instantaneous pressure drops in the region of z = 450 - 850 **mm**, where z is axial distance from the bottom of the rod bundle, were measured by using differential pressure transducers. The void fraction was evaluated from the pressure

drop neglecting the friction loss, which is much smaller than the density head.

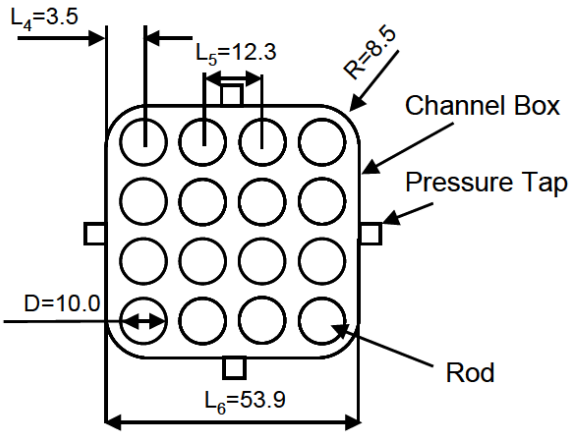

Fig.2 Horizontal cross section of rod bundle simulating part of PWR fuel assembly. (unit: **mm**)

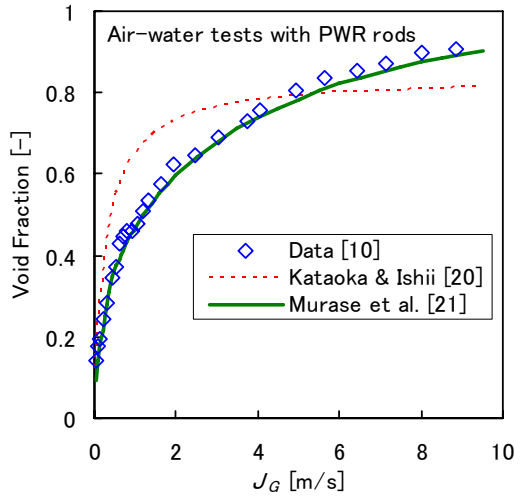

Fig.3 Void fractions in rod bundle simulating PWR fuels under stagnant liquid conditions.

Figure 3 shows the relationship between superficial air velocities and void fractions. As expected, the correlation by Kataoka and Ishii [20] does not agree with the data. The correlation proposed by Murase, *et al.* [21], which can be applied to circular tubes, annular channels and rod bundles, agrees well with the data.

$$\alpha = 0.037 Y^{1.68}, \quad \alpha \le 0.33 \qquad (1)$$

$$\left(1-\alpha^{1.45}\right) = \exp\left(-0.016 Y\right), \quad \alpha > 0.33 \qquad (2)$$

where

$$Y = \frac{1}{a\left(D_h^*\right)^{0.125}} \left(\frac{J_G}{\alpha}\right) \Bigg/ \left\{\frac{g\sigma\left(\rho_L-\rho_G\right)}{\rho_L^2}\right\}^{1/4} \qquad (3)$$

$$D_h^* = \frac{D_h}{\left\{\sigma / g\left(\rho_L-\rho_G\right)\right\}^{1/2}} \qquad (4)$$

$a = 1$ (for circular and rectangular tubes)

$a = 1.7$ (for rod bundles and annulus tubes)

In the equations, α is the average void fraction in the cross section, σ is the surface tension, ρ is the density, D_h is the hydraulic diameter, g is the gravity acceleration, and J is the superficial velocity. The subscripts, G and L, denote the gas and liquid, respectively.

2.4 Effects of non-condensable gas

The reflux condensation behavior in the SG tubes has been investigated using integral system test facilities [3-6]. In the riser section of tubes, the steam and non-condensable gas mixture and liquid condensate are in countercurrent flow. The condensation heat transfer coefficients in the presence of a non-condensable gas were measured in many experiments but very few measurements have been made in countercurrent flow. Therefore, experiments for reflux condensation heat transfer of steam-air mixtures were carried out at Purdue University under countercurrent flow in a vertical tube having an inside diameter of 19.3 **mm** and with a pressure range from 0.1 to 0.4 **MPa**, and an empirical correlation for the condensation heat transfer coefficients was obtained [15].

The condensation heat transfer coefficient, h_c, consists of the heat transfer coefficient of the liquid film, h_f, and the heat transfer coefficient at the gas-liquid interface, h_i. When the effects of the liquid film subcooling and the liquid film thickness on the gas-liquid interface area can be neglected, the condensation heat transfer coefficient is expressed by:

$$1/h_c = 1/h_f + 1/h_i \qquad (5)$$

In Eq. (5), the heat transfer coefficient of the liquid film, h_f, can be calculated by Nusselt's film condensation theory or an empirical correlation for a turbulent film, and the heat transfer coefficient at the gas-liquid interface, h_i, is obtained from the measured condensation heat transfer coefficient, h_c. The empirical correlation for the interfacial heat transfer coefficient was derived using the partial pressure ratio of steam and air, (P_{steam} /P_{air}), and the Reynolds

number of the steam-air mixture, Re_G. The derived empirical correlation is as follows:

$$Nu_i = 120\left(\frac{P_{steam}}{P_{air}}\right)^{0.75} \max(1.0, 0.0035 Re_G^{0.8}) \quad (6)$$

$$Nu_i = \frac{h_i D_{w,i}}{\lambda_G} \geq 4.36, \quad 0.0054 \leq \frac{P_{steam}}{P_{air}} \leq 120,$$

$$Re_G = \frac{J_G D_{w,i}}{\upsilon_G} \leq 10{,}000 \quad (7)$$

In Eq. (7), J_G is the superficial velocity of the steam-air mixture, $D_{w,i}$ is the inner diameter of the heat transfer tube, and ν_G is the kinematic viscosity of the steam-air mixture. The lower limit of the Nusselt number corresponds to the heat transfer of a gas laminar flow without steam condensation and gives h_i equal to about 7 **W/m^{2}K**. Other limits are due to the measured conditions. The derived correlation was implemented into RELAP5/MOD3. The temperature distributions of the steam-air mixture calculated with the improved correlation agreed well with the experimental data for different total pressures and inlet air flow rates [15].

In the test 7.2c using the BETHSY facility, which is a scale-model of a three-loop PWR, different flow patterns were observed in the 34 U-tubes [4]. In the test 7.2c/1.3, for example, an active condensation zone developed in the up-flow side of 21 U-tubes (active tubes), but a nitrogen gas flow from the outlet plenum to the inlet plenum occurred in some U-tubes (passive tubes). In order to evaluate the thermal-hydraulic behavior in SG U-tubes, flow patterns and condensation heat transfer in U-tubes were calculated using a one-dimensional parallel channel model (PCM) and RELAP5/MOD3 [16-17].

Figure 4 shows the calculated pressure drop between the inlet and outlet plenums in an average-length U-tube. The negative and positive gas flow rates show the nitrogen gas flow rate and the steam flow rate, respectively. Because the temperature of the steam-nitrogen gas mixture is higher and density head is lower in the hot side of the U-tube than in the cold side, the pressure drop becomes negative at low steam flow rates. In the U-tubes connected with the inlet and outlet plenums, each U-tube should have the same pressure drop. Therefore, three flow patterns of the high steam flow with active condensation, the low steam flow and the negative nitrogen gas flow with passive heat transfer may appear. In general, the flow in the region of the negative pressure drop gradient, dP/dW < 0, is unstable and is unlikely to appear. Therefore, the flow patterns of the high steam flow with active condensation and the negative nitrogen gas flow with passive heat transfer appear. At high steam flow rates, the pressure drop becomes positive because the friction loss is larger than the density head difference between the hot side and the cold side, and a single flow pattern appears in the U-tubes. The method to predict the ratio of active and passive U-tubes will be discussed later with the calculations using RELAP5/MOD3.

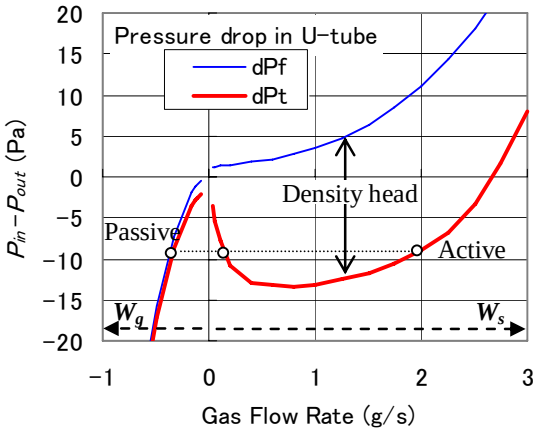

Fig.4 Pressure drop between inlet and outlet plenums in average-length U-tube.
(dPf: friction loss, dPt: total pressure drop)

Transient calculations were conducted using RELAP5/MOD3 with two or three flow channels for U-tubes. Figure 5 shows the nodalization scheme of RELAP5 for the SG of the BETHSY experiments with three flow channels, Volumes 115, 116 and 117. In the case of two flow channels, Volumes 115 and 116 were used. The nodalization used for these calculations included control volumes, junctions and heat structures. Volume 101 simulated the steam flow rate generated in the core. Volume 151 simulated the nitrogen flow injected into the hot leg. Volumes 10 and 15, and 90 and 95 were connected to the inlet plenum and the outlet plenum, respectively, in order to drain the condensate water, since the change in free volume affects the calculations. The water level in the secondary side of the SG was kept constant by feed

water from Volume 203. The pressure in the secondary side was kept at 0.2 **MPa**.

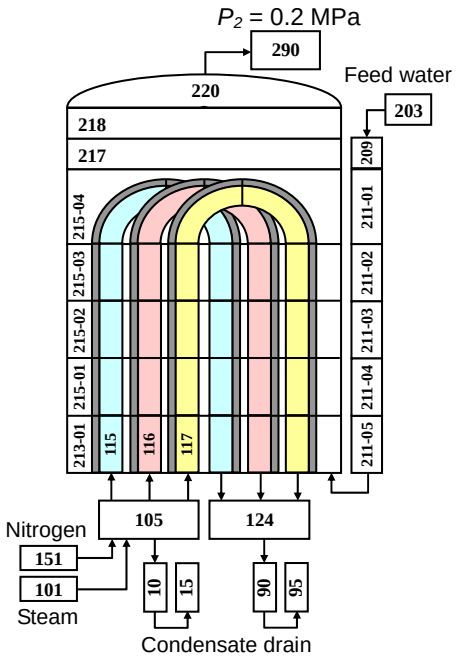

Fig.5 Nodalization for RELAP5 calculations.

Figure 6 shows the nitrogen gas recirculation flow rates in the case of two flow channels obtained by steady state calculations using the one-dimensional PCM and transient calculations using RELAP5. The number ratio of active tubes with steam condensation to passive tubes with the nitrogen gas reverse flow was given in the steady state calculations, but the number ratio of two flow channels was given in the transient calculations. The number ratio was the calculation parameter. In the PCM, there are no solutions with the same pressure drop between the active and passive tubes for some number ratios. On the other hand, in the RELAP5 calculations, the nitrogen gas reverse flow is not calculated in the two flow channels for some number ratios. In order to determine the most probable flow pattern shown in Fig. 6, the most stable state should be evaluated. The steam flow rate is too low and U-tubes have the surplus heat transfer area. Then, assuming that nitrogen gas re-circulated to supply a lack of the steam flow, the flow pattern with the maximum nitrogen gas recirculation flow rate would be the most stable state. Using the assumption, the numbers of the active tubes estimated by the PCM and RELAP5 are by one and three tubes larger than the data, respectively.

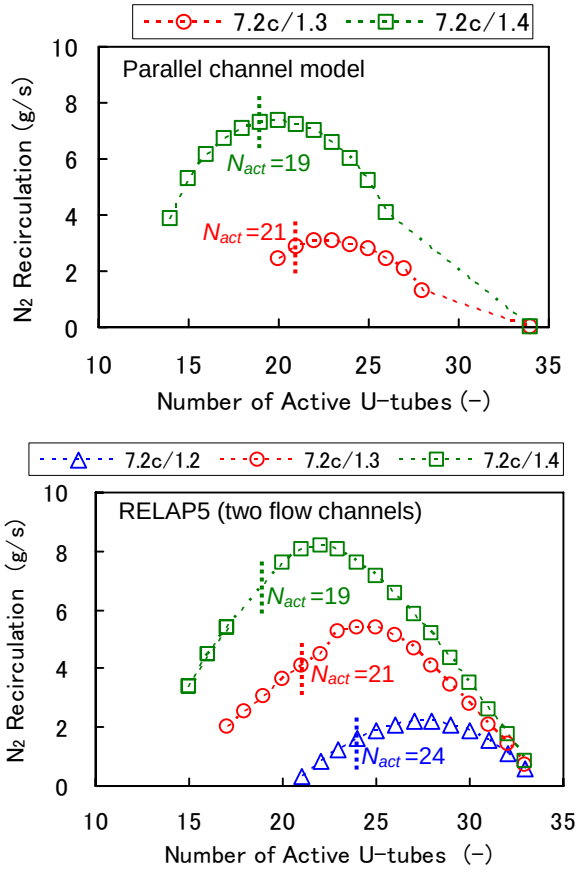

Fig.6 Nitrogen gas recirculation flow rates in 34 U-tubes. (N_{act}: observed number of active U-tubes [4])

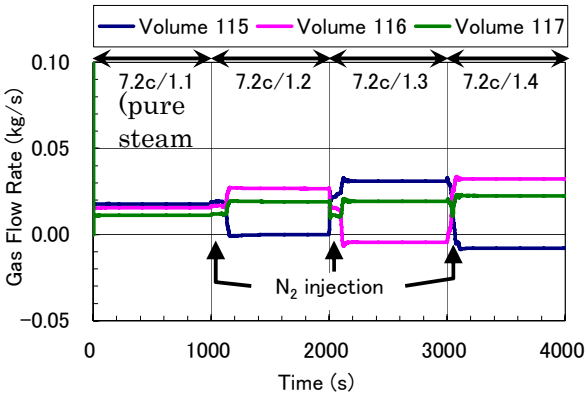

Fig.7 Gas flow rates at U-tube inlet in three flow-channels with 40, 35 and 25**%** flow area ratios.

As one typical example of RELAP5 calculations in three flow channels, Fig. 7 shows gas flow rates at the U-tube inlet. Flow area ratios of Volumes 115, 116 and 117 were 40, 35 and 25**%**, respectively. Due to nitrogen gas injection, nitrogen reverse flow appears in Volume 115 or 116, and the flow channel of nitrogen reverse flow changes during the transient.

Figure 8 compares predicted numbers of active U-tubes with the observed results [4]. In the calculations with two flow channels and the PCM, the assumption that the flow pattern with the maximum nitrogen gas recirculation flow rate would be the most stable was used in order to obtain unique solution. On the other hand, in the calculation with three flow channels, the assumption was not used. In that case, calculations are not stable and calculated results depend on the flow area ratios. Therefore, in order to obtain reliable results, it is desirable to calculate several cases with different flow area ratios and obtain the average value of the several cases. The predicted values agree well with the data except for test 7.2c/1.2 with a small amount of nitrogen gas. The results indicate that the assumption of the maximum nitrogen gas recirculation flow rate is valid and that the transient calculation with three flow channels gives the number of active U-tubes without the assumption.

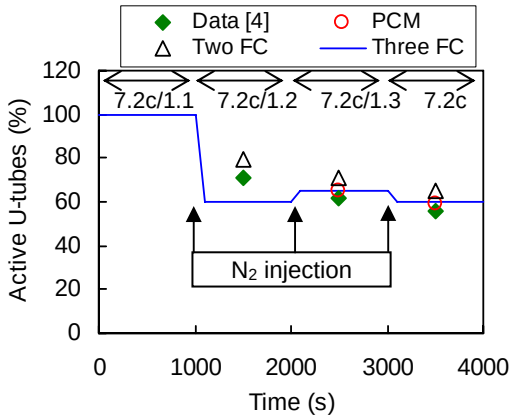

Fig.8 Comparison of active U-tubes. (FC: flow channels)

In this study, the mechanism of non-condensable gas recirculation in SG U-tubes was evaluated and the prediction method of the ratio of active and passive U-tubes was proposed. The correlation for condensation heat transfer greatly affected calculations of temperature distributions and the prediction for the ratio of active and passive U-tubes. However, the correlation for condensation heat transfer and non-condensable gas recirculation did not greatly affect the RCS pressure [16], because the condensing region in the SG U-tubes was only about 20**%** of the U-tube length.

2.5 CCFL in a surge line

Takeuchi, *et al.* [22] evaluated CCFL characteristics in the pressurizer surge line using the Taitel-Dukler model on flow pattern transitions for the slightly inclined horizontal pipes and the existing CCFL correlations for vertical pipes. However, the validation of their results is not sufficient, because CCFL data in the pressurizer surge line are quite limited. Therefore, air-water tests have been carried out at Kobe University [18].

Figure 9 shows the test apparatus for the measurements of CCFL in the pressurizer surge line. Air and water at atmospheric pressure and room temperature are used for the gas and liquid phases. The apparatus consists of air and water supply systems, an upper tank simulating the pressurizer, a surge line, a part of a hot leg, and a lower tank simulating the upper plenum in the RV. The test section and the upper and lower tanks are made of transparent acrylic resin to observe flow patterns. The inner diameter of the surge line is 30 **mm**, which is about 1/10-scale of a PWR surge line. The inclination angle of the slightly inclined horizontal pipe, θ, can be continuously changed.

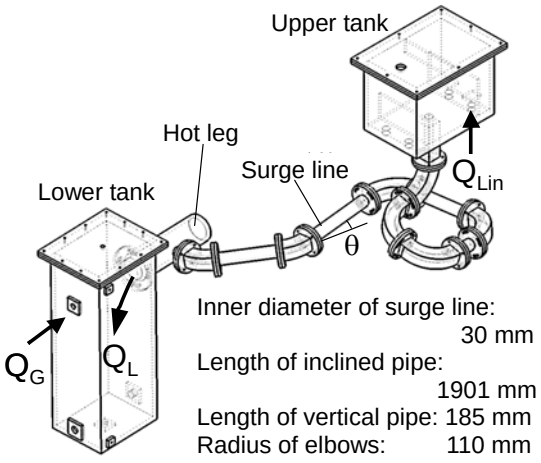

Fig.9 CCFL test apparatus in surge line.

Figure 10 shows the measured CCFL characteristics in the surge line, which are expressed using Wallis parameters [23].

$$J_k^* = J_k / \{gD(\rho_L - \rho_G)/\rho_k\}^{1/2}, (k = G, L) \quad (8)$$

where J_k is the superficial velocity of phase-*k* in the surge line, and the characteristic length is the inner

diameter, *D*. The falling water flow rate was limited at either the upper junction (CCFL-U), the inclined pipe (CCFL-S) or the lower junction (CCFL-L). The smaller the inclination of the surge line was, the stronger the effect of inclination on CCFL was.

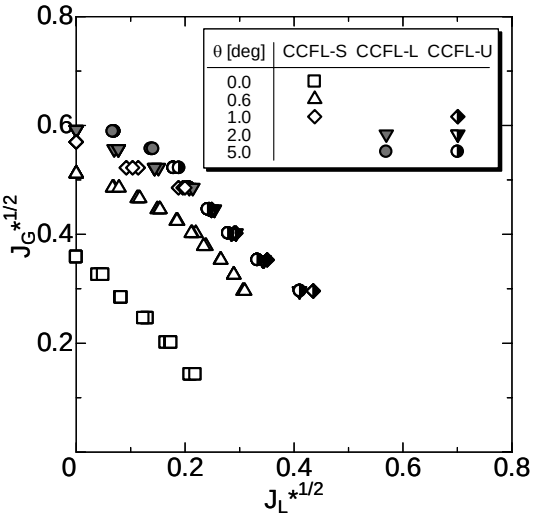

Fig.10 CCFL characteristics measured in surge line [18].

CCFL characteristics are generally expressed by the Wallis correlation [23]:

$$\sqrt{J_G^*} + m\sqrt{J_L^*} = C\,, \qquad (9)$$

where m and C are empirical constants. For CCFL-S and CCFL-L in the slightly inclined horizontal pipes, the effects of pipe diameters can be expressed by the Wallis parameters, which will be discussed in section 3. For CCFL-U in vertical pipes, however, it is well known that the effects of pipe diameters cannot be expressed by the Wallis parameters. For vertical pipes with large diameters, the Laplace capillary length should be used for the characteristic length in Wallis parameters. The Laplace capillary length used as the characteristic length in the Wallis parameters leads to the Kutateladze numbers, K_k, and another CCFL correlation, given by:

$$\sqrt{K_G^*} + m_K\sqrt{K_L^*} = C_K\,, \qquad (10)$$

$$K_k^* = J_k \Big/ \left\{ g\sigma\left(\rho_L - \rho_G\right)/\rho_k^2 \right\}^{1/4},\ (k = G, L) \qquad (11)$$

where m_K and C_K are empirical constants. In a PWR surge line with the inner diameter of about 300 **mm**, CCFL-U becomes critical and Eq. (10) can be used for the CCFL correlation except in the region of large J_G.

3 Countercurrent flows in a hot leg

In RELAP5, gas-liquid two-phase flows are calculated using flow pattern maps and gas-liquid interfacial drag correlations for each flow pattern. For inclined pipes, flow patterns are generally selected from those in horizontal pipes or vertical pipes, based on the inclination angle.

The PWR hot leg consists of a horizontal pipe, an elbow and an inclined pipe with the inclination angle of 50°, where the flow pattern map in vertical pipes is generally used. A number of experiments have been conducted on the CCFL characteristics in a hot leg. On the other hand, few observations of flow patterns have been reported. Therefore, air-water tests were carried out at Kobe University using a 1/5-scale model with a rectangular cross section [11] and a 1/15-scale model with a circular cross section [12], and numerical simulations for the tests were conducted using a two-fluid model in a thermal-hydraulic analysis code FLUENT6.3.26 [13-14].

3.1 1/5-scale tests with rectangular channel

Figure 11 shows the test apparatus for countercurrent flow in the hot leg [11]. Air and water at atmospheric pressure and room temperature are used for the gas and liquid phases. The apparatus consists of air and water supply systems, an upper tank simulating the inlet plenum of the SG, a hot leg, and a lower tank simulating the RV. Water is pumped from the reservoir to the upper tank through a flow meter. Air is injected from a compressor to the lower tank through a regulator and a flow meter. Injected water and air form a countercurrent flow in the hot leg. Water flows into the lower tank and overflows into the upper tank, and then returns to the reservoir through each drain line. The test section, shown in Fig. 12, is made of transparent acrylic resin to allow observation of flow patterns. Three air supply tubes are connected to the lower tank on the opposite side of the hot leg to investigate the effects of air supply conditions. The hot leg has a rectangular cross section with a 10 **mm** width and 150 **mm** height. The height of 150 **mm** is about 1/5 of the diameter of the PWR hot leg, and the inclination of the inclined pipe is 50°.

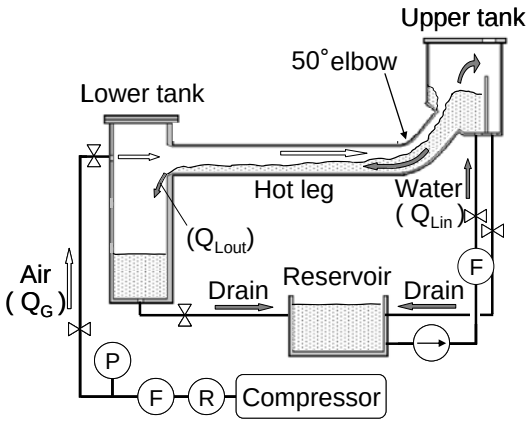

P: Pressure gauge, F: Flow meter, R: Regulator

Fig.11 Test apparatus for countercurrent flow in hot leg.

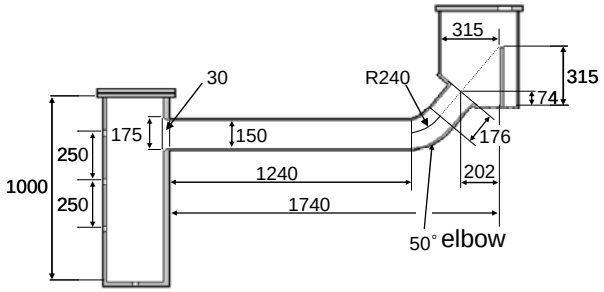

Fig.12 Test section of 1/5-scale model with rectangular channel. (unit: **mm**)

A flow pattern diagram was obtained by keeping the injected water flow rate (Q_{Lin}) constant, while the air flow rate (Q_G) was gradually increased in order to investigate flow pattern transitions in the horizontal, elbow and inclined sections. The top air supply tube was used. In the high gas flow rate conditions, the water flow into the lower tank (Q_{Lout}) was less than Q_{Lin} because some injected water returned to the upper tank and overflowed. A Hi-vision video camera and a high speed camera were used to record flow patterns.

In the CCFL measurements, water was supplied to the upper tank at a constant flow rate Q_{Lin}. Air was supplied to the lower tank through the top tube and gradually increased until water overflowed in the upper tank. The water flow rate Q_{Lout} drained into the lower tank through the test section was measured from the increasing rate of the water level in the lower tank for each air flow rate Q_G. From the test condition of Q_G and the measured value of Q_{Lout}, air and water superficial velocities in the test section, J_G and J_L, were calculated. Then the relationship between $(J_G^*)^{0.5}$ and $(J_L^*)^{0.5}$ was correlated using the Wallis parameters expressed by Eq. (8).

3.2 1/15-scale tests with circular pipe

In the tests using the 1/15-scale model of a PWR hot leg with the inner diameter of 50 **mm**, the test apparatus was similar to the 1/5-scale model apparatus shown in Fig. 11. Figure 13 shows the test section of the 1/15-scale model [12] made of transparent acrylic resin to allow observation of flow patterns. In the CCFL measurements, water was supplied to the upper tank at a constant flow rate Q_{Lin}. Air was supplied to the lower tank. Air flow rate was gradually increased until the water flow rate, Q_{Lout}, became zero and gradually decreased until deflooding occurred.

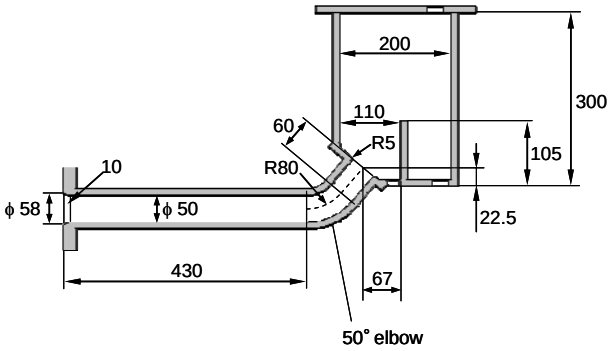

Fig.13 Test section of 1/15-scale model. (unit: **mm**)

3.3 Numerical method

Wang, *et al.* [24] conducted two-dimensional analyses of countercurrent flows in the hot leg of the UPTF tests [25] using a two-fluid model. In two-dimensional analyses, the effects of wall friction cannot be correctly evaluated. And Wang, *et al.* assigned boundary conditions at the inlet and outlet of the hot leg, which might affect the calculated flow patterns in the hot leg. The CCFL characteristics cannot be calculated using boundary conditions given at the inlet and outlet of the hot leg. Therefore, in this study, three-dimensional calculations including the lower and upper tanks were conducted.

The two-fluid model in the thermal-hydraulic analysis code FLUENT6.3.26 was used. The $k-\varepsilon$ turbulent model was used for the gas and liquid phases in order to simulate turbulent velocity distributions. Momentum, volume fraction, turbulent kinetic energy

and turbulent dissipation rate of the gas and liquid phases were calculated using the first order upwind scheme. The phase-coupled-SIMPLE method was used for the pressure-velocity coupling.

In the two-fluid model, a user function to calculate the interfacial drag coefficients was employed. In the momentum equation, the interfacial friction force F_{km} [**N/m^3**] is defined by:

$$F_{km} = -0.5 C_D \rho_c |u_r| u_r A_i \qquad (12)$$

where ρ_c is the density of the continuous phase and $\rho_c = \rho_G$ was used. C_D is the interfacial drag coefficient, u_r is the relative velocity of the gas and liquid phases, and A_i [**m^2/m^3**] is the interfacial area concentration. The interfacial drag coefficient, ($C_D A_i$), applicable to three-dimensional calculations has not been established. Therefore, various combinations of correlations developed for the one- dimensional two-fluid model were tested, and a combination of correlations, which gave the best agreement with the experiments, was selected [26]. The resulting combination is given by the following three correlations as a function of local void fractions:

$$C_D A_i = \min\left[(C_D A_i)_B, \max\left\{(C_D A_i)_S, (C_D A_i)_A\right\}\right] \qquad (13)$$

$$(C_D A_i)_B = 2\alpha(1-\alpha) g / V_{gj}^2 \qquad (14)$$

$$(C_D A_i)_S = 9.8(1-\alpha)^3 \left\{\frac{4.5\alpha}{D_h}\right\} \qquad (15)$$

$$(C_D A_i)_A = 0.02\{1 + 75(1-\alpha)\}\alpha^{0.5} / D_h \qquad (16)$$

where V_{gj} is the drift velocity, and D_h is the hydraulic diameter. Equation (14) is proposed by Andersen [27] based on the drift-flux model. Minato, *et al.* [28] used Eq. (14) with the correlation of drift velocity proposed by Ishii [29] in the region of $0 \le \alpha \le 1$, and obtained good results in the calculations using the two-fluid model especially for co-current up-flows. The correlation, however, gives large drag coefficients for countercurrent flows and in the region of high void fractions. For countercurrent flows, it is better to use the correlation of drift velocity for stagnant liquid, and the following correlation was used.

$$V_{gj} = 1.4\left(D_h^*\right)^{0.125}\left\{\frac{g\sigma(\rho_L - \rho_G)}{\rho_L^2}\right\}^{1/4}, \qquad (17)$$

$$D_h^* = D_h\left\{\frac{g(\rho_L - \rho_G)}{\sigma}\right\}^{1/2} \qquad (18)$$

Equation (17) is simplified from the original correlation proposed by Kataoka, *et al.* [30]. In the region of high void fractions, Eqs. (15) and (16) were used, respectively, for slug flow [31] and annular flow [23]. Equation (15) is simplified from the original correlation by assuming $\alpha_{gs} = 0$.

Figure 14 shows the computational grid for the 1/5-scale tests with a rectangular cross section [13]. Because velocity distributions of gas and liquid at the both ends of the hot leg affect hydraulic behavior, the calculation region includes the lower and upper tanks. The total number of calculation cells is about 140,000.

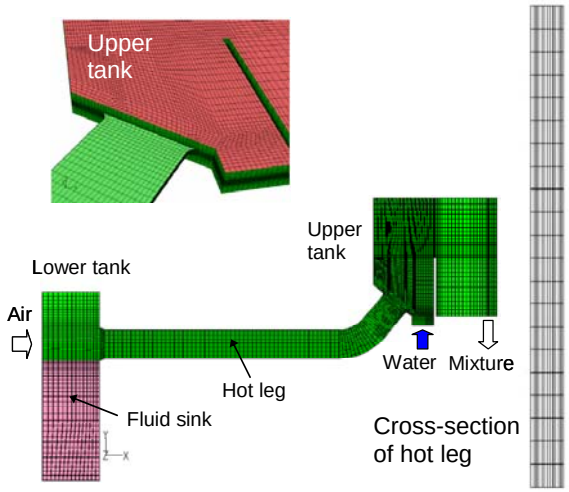

Fig.14 Computational grid for 1/5-scale tests.

Figure 15 shows the computational grid for the 1/15-scale tests [14]. The calculation region includes the upper and lower tanks to calculate CCFL characteristics and the total number of calculation cells is about 70,000.

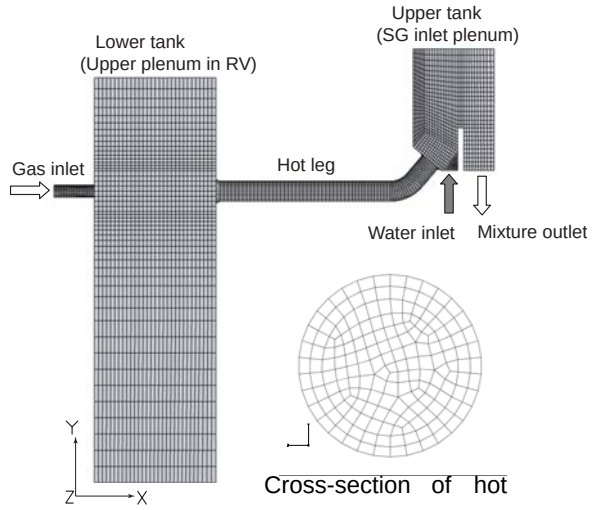

Fig.15 Computational grid for 1/15-scale tests.

In both calculations for the 1/5-scale and 1/15-scale models, water is supplied from the bottom of the upper tank. Some water gravitationally flows into the lower tank through the hot leg. The water flow rate through the hot leg is calculated from the mass increasing rate in the lower tank. The rest of the water, which does not flow into the lower tank, overflows the barrage in the upper tank and flows out with the air through the mixture outlet. Boundary conditions are constant velocity at inlets of air and water and constant pressure at the mixture outlet.

3.4 Results on the 1/5-scale model

In the Wallis parameters expressed by Eq. (8), the channel height of H = 150 **mm** was used for the characteristic length. Test parameters were the injected water flow rate and air flow rate, which were J_{Lin} = 0.011 - 0.17 **m/s** ($(J_{Lin}^*)^{0.5}$ =0.10 - 0.37) and J_G = 3.4 - 10.7 **m/s** ($(J_G^*)^{0.5}$ = 0.31 - 0.55), respectively [11]. Figure 16 shows flow pattern transitions and CCFL characteristics, and Fig. 17 shows flow patterns.

By increasing J_G^* at a constant J_{Lin}^*, the flow pattern changed from stratified flow to wavy flow, flooding occurred in the horizontal section near the elbow, and just after the flooding initiation, the flow pattern changed to wavy mist flow. Therefore, the boundary between wavy and wavy mist flows agreed well with the CCFL characteristics. It was confirmed that there were no differences in CCFL characteristics between the increasing and decreasing processes of air flow rates, and that hysteresis did not appear.

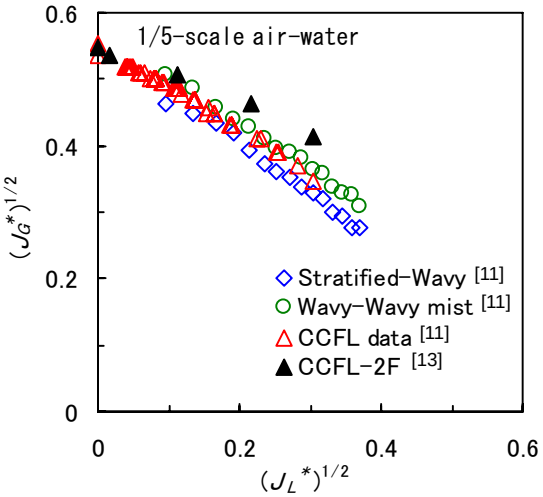

Fig.16 Flow pattern transitions and CCFL characteristics.
(2F: two-fluid model)

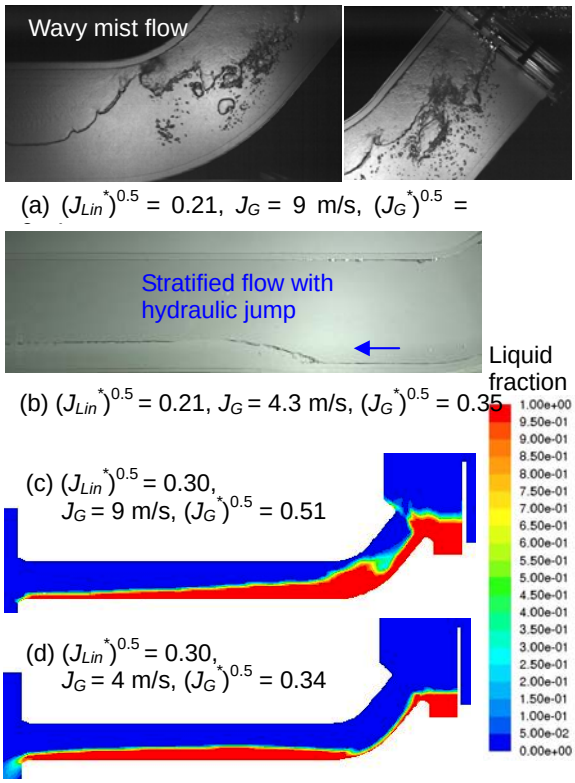

Fig.17 Observed and calculated flow patterns.

Calculated flow patterns were similar to the observed ones as shown in Fig. 17, but wavy flow was not obtained due to the large calculation cells. Calculated J_G^* at J_L^* = 0 agreed very well with the measured value as shown in Fig. 16. However, the calculations underestimated the slope, *i.e.* the constant m in Eq. (9).

3.5 Results on the 1/15-scale model

Test parameters were the injected water flow rate and air flow rate, which were J_{Lin} = 0.042 - 0.26 **m/s** ($(J_{Lin}^*)^{0.5}$ = 0.25 - 0.61) and J_G = 0 - 7.4 **m/s** ($(J_G^*)^{0.5}$ = 0 - 0.61), respectively [12]. Figure 18 shows CCFL characteristics and Fig. 19 shows flow patterns in the case of J_{Lin} = 0.17 **m/s**.

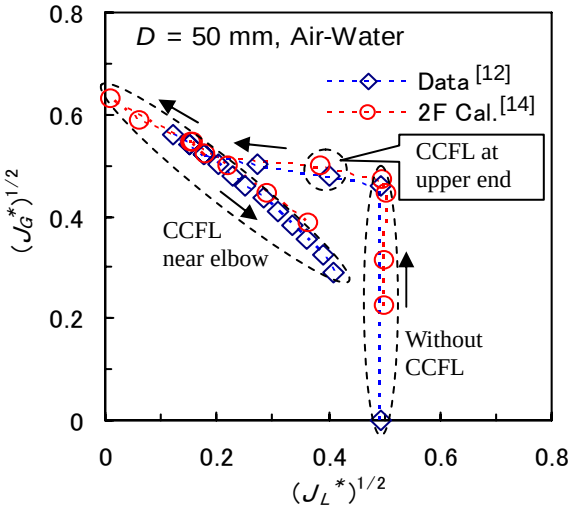

Fig.18 CCFL characteristics.
(J_{Lin} = 0.17 **m/s**, 2F: two-fluid model)

In the process of increasing the air flow rates, all the injected water flowed through the hot leg in the region of J_G < 4.4 **m/s**, and the flow pattern was stratified flow in the horizontal, elbow and inclined sections (c.f. Fig. 19 (a)). At J_G = 4.8 **m/s**, the water flow rate was restricted at the upper end of the inclined pipe. The flow pattern did not change in the horizontal and elbow sections, but it did in the upper part of the inclined pipe where it changed from stratified flow to annular flow (c.f. Fig. 19 (b)), as the annular liquid film flowed downward from the upper tank. At J_G = 5.6 **m/s**, flow patterns changed, and were wavy flow, wavy mist flow and annular mist flow in the horizontal, elbow and inclined sections, respectively (c.f. Fig. 19 (c)). Then, the water flow rate was restricted near the elbow in the horizontal pipe. In the elbow and inclined pipe, large waves with droplets periodically flowed upward, water flowed downward from the upper tank, and recirculation of water with bubbles and droplets formed. Therefore, flow pattern fluctuated in the elbow and inclined pipe.

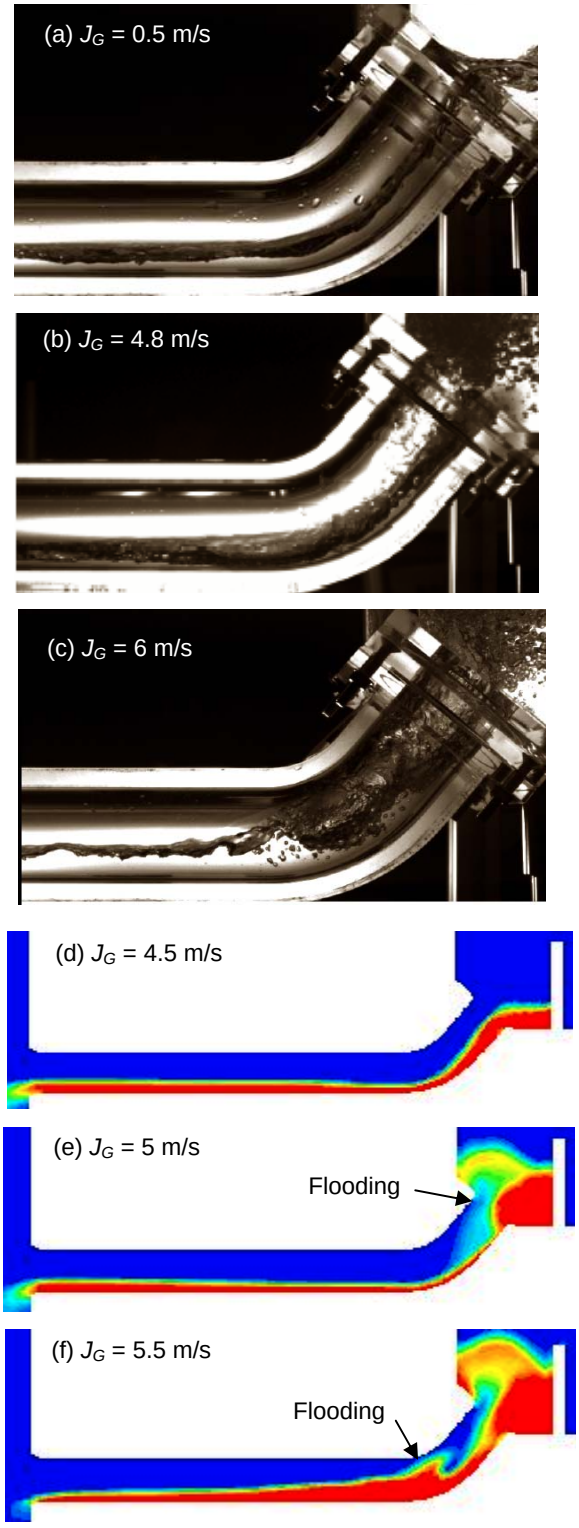

Fig.19 Observed and calculated flow patterns.
(J_{Lin} = 0.17 **m/s**, Liquid fraction: see Fig. 17)

In the course of decreasing air flow rates, however, the same flow patterns of wavy flow, wavy mist flow and annular mist flow continued. Therefore, CCFL characteristics were different between the increasing and decreasing processes of air flow rates, and showed hysteresis.

Calculated flow patterns were similar to observed ones except for the small waves and liquid film on the upper part of the inclined pipe, which could not be calculated due to the large calculation cells. The calculated CCFL characteristics agreed very well with the data including hysteresis.

In the course of increasing air flow rates, first the water flow rate through the hot leg was restricted at the upper end of the inclined pipe as shown in Figs. 19 (b) and (e). In the test section shown in Fig. 13, however, the expansion of the inclined pipe in a PWR hot leg was not simulated. The expansion mitigates CCFL there and CCFL at the upper end of the inclined pipe may not appear in the PWR hot leg.

3.6 Scale effects on CCFL characteristics

Navarro [32] observed similar hysteresis to that shown in Fig. 18 using an air-water system with the inner diameter of 54 mm. In most of CCFL tests simulating a PWR hot leg, however, the hysteresis between increasing and decreasing processes of gas flow rates has not been reported like the 1/5-scale tests in this study. In a large system, waves grow to become large rolling waves in the horizontal section and the flow patter transition from wavy flow to wavy mist flow may easily occur (c.f. Fig. 16). Therefore, the hysteresis may not appear in PWR conditions, and CCFL characteristics in the decreasing process of gas flow rate might be important to evaluate countercurrent flow in the PWR hot leg.

Figure 20 shows the effects of pipe diameter on CCFL characteristics calculated using FLUENT 6.3.26 and the two-fluid model [33]. The figure shows that the effects of diameter can be expressed by the Wallis parameters, Eq. (8).

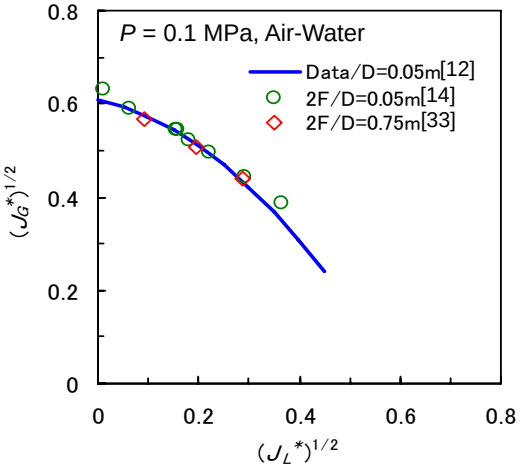

Fig.20 Effects of diameters on CCFL characteristics.

A number of experiments have been conducted on the CCFL characteristics in a hot leg. However, the specifications of the test sections are different and CCFL characteristics cannot be directly compared. Table 2 lists conditions in some of CCFL tests, which are similar, and Fig. 21 compares CCFL characteristics. CCFL characteristics in this study agree very well with those by Navarro [32], and agree well with those by Geffraye, *et al.* [34] and UPTF data [25] except in the region of large J_G^*. One of the major parameters is the ratio of the horizontal length to the diameter, L_H/D. As expressed by data of Richter, *et al.* [35], the smaller L_H/D is, the more mitigated CCFL is.

Figure 21 shows that CCFL characteristics in the PWR hot leg can be expressed by Wallis parameters for different diameters and fluid properties. On the other hand, both air-water and steam-water CCFL tests were carried out at Forschungszentrum Dresden-Rossendorf (FZD) using the 1/3-scale rectangular channel (channel height of H = 0.25 **m**) simulating the PWR hot leg, and the results revealed a clear difference between the air-water tests at 0.15 and 0.3 **MPa** and the steam-water tests at 1.5, 3 and 5 **MPa** [36], when the CCFL data were plotted in terms of the Wallis parameters. Therefore, the effects of fluid properties on CCFL characteristics in the hot leg have not been clarified especially for high pressure and high temperature conditions.

Table 2 Conditions of CCFL tests simulating a PWR hot leg

	D [**m**]	L_H/D	Fluid/ P [**MPa**]
This study	0.050	8.6	A-W/ 0.1
Navarro [32]	0.054	1.9-15	A-W/ 0.1
Richter [35]	0.203	4.5	A-W/ 0.1
Geffraye [34]	0.351	7.5	A-W/ 0.1
UPTF [25]	0.750	9.0	S-W/ 1.5

L_H: length of horizontal section, A: air, S: steam, W: water

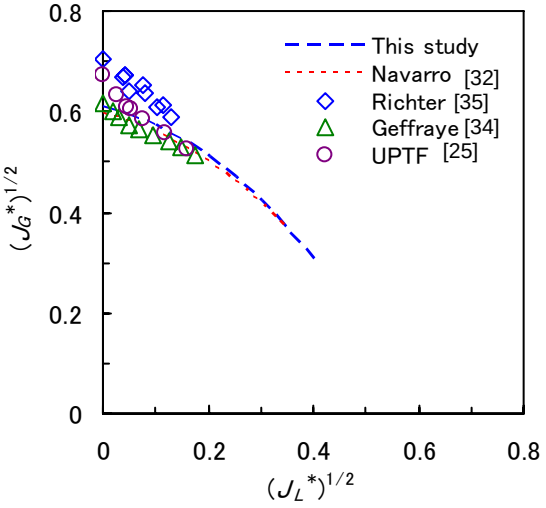

Fig.21 Comparison of CCFL characteristics.

4 Concluding remarks

The loss-of-RHR during mid-loop operation is one of the relatively high-risk events in PWRs. In order to increase reliability of transient analyses, the CSAU methodology has been applied to evaluate the loss-of-RHR event, and the PIRT for the event has been developed. Based on the PIRT, important thermal-hydraulic behaviors during a loss-of-RHR event have been evaluated. As one of substitute methods of RHR cooling, reflux condensation by a SG is expected to be applicable. In that case, behavior of non-condensable gas (*i.e.* air) in the RCS and countercurrent gas-liquid flow in the hot leg affect heat transfer in the SG U-tubes, RCS pressure and coolant level in the core.

Condensation heat transfer experiments in the presence of non-condensable gas were carried out at Purdue University, and an empirical correlation for condensation heat transfer in the SG tubes was derived. Also the mechanism of non-condensable gas recirculation in SG U-tubes, which was observed in the BETHSY experiments, was evaluated, and BETHSY test analyses were conducted using RELAP5/MOD3 with the improved correlation. The predicted ratio of active U-tubes with steam condensation and passive U-tubes with non-condensable gas recirculation agreed with the observed values.

As for countercurrent gas-liquid flow in the hot leg, which consists of horizontal, elbow and inclined sections, air-water experiments were carried out at Kobe University using the 1/5-scale model with a rectangular channel of 150 **mm** height and the 1/15-scale model with the inner diameter of 50 **mm**, and numerical simulations were conducted using a two-fluid model in the thermal-hydraulic analysis code FLUENT6.3.26, in order to evaluate flow patterns and CCFL characteristics. The calculated flow patterns in the hot leg were quite similar to the observed results, and the calculated CCFL characteristics agreed well with the data. Flow patterns in the hot leg, which were split by the CCFL curve, were stratified flow without CCFL and wavy mist flow under CCFL conditions. CCFL characteristics were suitably expressed by the Wallis parameters under the low pressure conditions.

Nomenclature

A_i interfacial area concentration [**m^2/m^3**]
C constant in Wallis correlation [-]
C_D interfacial drag coefficient [-]
D diameter [**m**]
D_h hydraulic diameter [**m**]
D^* dimensionless diameter [-]
g acceleration of gravity [**m/s^2**]
h heat transfer coefficient [**W/m^{2}K**]
J superficial velocity [**m/s**]
J^* dimensionless superficial velocity [-]
K^* dimensionless superficial velocity [-]
L_H horizontal length of hot leg [**m**]
m constant in Wallis correlation [-]
P pressure [**Pa**]
u_r relative velocity [**m/s**]
V_{gj} drift velocity [**m/s**]

Greek symbols

α void fraction [-]

ρ density [**kg/m^3**]
σ surface tension [**N/m**]

Subscripts

c condensation or continuous-phase
f film
G gas
i interface
L liquid

References

[1] USNRC: Loss of Residual Heat Removal System Diablo Canyon Unit 2 April 10, 1987, NUREG-1269, Washington, D. C., US Nuclear Regulatory Commission, 1987.

[2] USNRC: Loss of Vital AC Power and the Residual Heat Removal System During Mid-loop Operations at Vogtle Unit 1 on March 20, 1990, NUREG-1410, Washington, D. C., US Nuclear Regulatory Commission, 1990.

[3] NAKAMURA, H., KATAYAMA, J., KUKITA, Y.: Loss of Residual Heat Removal (RHR) Event during PWR Mid-loop Operation: ROSA-Ⅳ/LSTF Experiment without Opening on Primary Loop Pressure Boundary, FED ASME Power Plant Transients, 1992, 140: 9-16.

[4] DUMONT, D., LAVIALLE, G., NOEL, B., DERUAZ, R.: Loss of Residual Heat Removal during Mid-loop Operation: Bethsy Experiment, Nuclear Eng. and Design, 1994, 149: 365-374.

[5] MANDL, R., UMMINGER, K., LOGT, J.: Failure of PWR-RHRs under Cold Shutdown Conditions Experimental Results from the PKL Test Facility, Proceedings of 18th Water Reactor Safety Research Information Meeting, Rockville, MD, 1990: 329-351.

[6] LEE, C., LIN, T., WAY, Y., HSIA, D: Investigation of Mid-loop Operation with Loss of RHR at Iner Integral System Test (IIST) Facility, Nuclear Eng. and Design, 1996, 163: 349-358.

[7] NAFF, S. A., JOHNSEN, G. W., PALMROSE, D. E., HUGHES, E. D., KULLBERG, C. M., ARCIERI, W. C.: Thermal-hydraulics Processes during Reduced Inventory Operation with Loss of Residual Heat Removal, NUREG/CR- 5855, Washington, D. C., US Nuclear Regulatory Commission, 1992.

[8] BOYACK, B., *et al.*: Quantifying Reactor Safety Margins, Application of Code Scaling, Applicability and Uncertainty Evaluation Methodology to a Large-break, Loss-of-coolant Accident, NUREG/CR-5249, Washington, D. C., US Nuclear Regulatory Commission, 1989.

[9] NAGUMO, H., SASAKI, Y., MURASE, M., YOSHIDA, Y.: Development of PIRT and Verification of RELAP5 Void Model for Application to the Loss-of-RHR Event during Mid-loop Operation, Proceedings of 16th Int. Conference on Nuclear Eng., ICONE16-48064, Orlando, USA, 2008.

[10] KAMEI, A., HOSOKAWA, S., TOMIYAMA, A., KINOSHITA, I., MURASE, M.: Void Fraction in a Four by Four Rod Bundle under a Stagnant Condition, J. of Power and Energy Systems, 2010, 4 (2): 315-326.

[11] MINAMI, N., NISHIWAKI, D., KATAOKA, H., TOMIYAMA, A., HOSOKAWA, S., MURASE, M.: Countercurrent Gas-liquid Flow in a Rectangular Channel Simulating a PWR Hot Leg (1); Flow Pattern and CCFL Characteristics, Japanese J. of Multiphase Flow, 2008, 22 (4): 403-412. [in Japanese]

[12] MINAMI, N., NISHIWAKI, D., NARIAI, T., TOMIYAMA, A., MURASE, M.: Countercurrent Gas-liquid Flow in a PWR Hot Leg under Reflux Cooling (I) Air-water Test for 1/15th Scale Model of a PWR Hot Leg, J. Nucl. Sci. Technol., 2010, 47 (2): 142-148.

[13] MINAMI, N., MURASE, M., NISHIWAKI, D., TOMIYAMA, A.: Countercurrent Gas-liquid Flow in a Rectangular Channel Simulating a PWR Hot Leg (2); Analytical Evaluation of Countercurrent Flow Limitation, Japanese J. of Multiphase Flow, 2008, 22 (4): 413-422. [in Japanese]

[14] MINAMI, N., MURASE, M., TOMIYAMA, A.: Countercurrent Gas-liquid Flow in a PWR Hot Leg under Reflux Cooling (II) Numerical Simulation of 1/15-SCALE Air-water Tests, J. Nucl. Sci. Technol., 2010, 47 (2): 149-155.

[15] NAGAE, T., MURASE, M., CHIKUSA, T., VIEROW, K., WU., T.: Reflux Condensation Heat Transfer of Steam-air Mixture under Turbulent Flow Conditions in a Vertical Tube, J. Nucl. Sci. Technol., 2007, 44 (2): 171-182.

[16] NAGAE, T., CHIKUSA, T., MURASE, M., MINAMI, N.: Analysis of Noncondensable Gas Recirculation Flow in Steam Generator U-tubes during Reflux Condensation Using RELAP5, J. Nucl. Sci. Technol., 2007, 44 (11): 1395-1406.

[17] MINAMI, N., CHIKUSA, T., MURASE, M.: RELAP5 Analysis of Thermal-hydraulic Behavior in Steam Generator U-tubes during Reflux Condensation, Nuclear Technology, 2008, 164: 265-277.

[18] FUTATSUGI, T., NARIAI, T., TOMIYAMA, A., KINOSHITA, I., MURASE, M.: Study on Counter-current Flows in Scale Down Model of a PWR Surge Line, JSMF Annual Meeting 2010, D342, Hamamatsu, Japan, 2010. [in Japanese]

[19] UTANOHARA, Y., MURASE, M.: Numerical Analysis of Steam-air Behavior in a Pressurizer during Reflux Cooling, Proceedings of 6th Japan-Korea Symposium on Nuclear Thermal Hydraulics and Safety, N6P1018, Okinawa, Japan, 2008.

[20] KATAOKA, I., ISHII, M.: Drift-flux Model for Large Diameter Pipe and New Correlation for Pool Void Fraction, Int. J. of Heat and Mass Transfer, 1987, 30: 1927-1939.

[21] MURASE, M., SUZUKI, H., MATSUMOTO, T., NAITOH, M.: Countercurrent Gas-liquid Flow in Boiling ChannelS, J. Nucl. Sci. Technol., 1986, 23 (6): 487-502.

[22] TAKEUCHI, K., YOUNG, M. Y., GAGNON, A. F.: Flooding in the Pressurizer Surge Line of AP600 Plant and

Analyses of Apex Data, Nuclear Eng. and Design, 1999, 192: 45-58.

[23] WALLIS, G. B.: One-dimensional Two-phase Flow, New York: McGraw Hill, 1969: 320-339.

[24] WANG, M. J., MAYINGER, F.: Simulation and Analysis of Thermal-hydraulic Phenomena in a PWR Hot Leg Related to SBLOCA, Nuclear Eng. and Design, 1995, 155: 643-652.

[25] MAYINGER, F., WEISS, P., WOLFERT, K.: Two-phase Flow Phenomena in Full-scale Reactor Geometry, Nuclear Eng. and Design, 1993, 145: 47-61.

[26] UTANOHARA, Y., KINOSHITA, I., MURASE, M., MINAMI, N., TOMIYAMA, A.: Effects of Interfacial Friction Correlations on Numerical Calculations for Countercurrent Gas-liquid Flow in a PWR Hot Leg, Proceedings of the 13th Int. Topical Meeting on Nuclear Reactor Thermal Hydraulics, N13P1101, Kanazawa, Japan, 2009.

[27] ANDERSEN, J. G. M.: Interfacial Shear for Two-fluid Models, American Nuclear Society Transactions, 1982, 41: 669-671.

[28] MINATO, A., TAKAMORI, K., ISHIDA, N.: An Extended Two-fluid Model for Interface Behavior in Gas-liquid Two-phase Flow, Proceedings of 8th Int. Conf. on Nuclear Eng., No. 8045, Baltimore, MD, USA, 2000.

[29] ISHII, M.: One-dimensional Drift-flux Model and Constitutive Equations for Relative Motion Between Phases in Various Two-phase Flow Regimes, ANL-77-47, Argonne, IL, Argonne National Laboratory, 1977.

[30] KATAOKA, Y., SUZUKI, H., MURASE, M.: Drift- flux Parameters for Upward Gas Flow in Stagnant Liquid, J. Nucl. Sci. Technol., 1987, 24 (7): 580-586.

[31] ISHII, M., MISHIMA, K.: Two-fluid Model and Hydro-dynamic Constitutive Relations, Nuclear Eng. and Design, 1984, 82: 107-126.

[32] NAVARRO, M. A.: Study of Countercurrent Flow Limitation in a Horizontal Pipe Connected to an Inclined One, Nuclear Eng. and Design, 2005, 235: 1139-1148.

[33] KINOSHITA, I., UTANOHARA, Y., MURASE, M., MINAMI, N., TOMIYAMA, A.: Numerical Calculations on Countercurrent Gas-liquid Flow in a PWR Hot Leg (2) Steam-water Flow under PWR Plant Condition, Proceedings of the 13th Int. Topical Meeting on Nuclear Reactor Thermal Hydraulics, N13P1040, Kanazawa, Japan, 2009.

[34] GEFFRAYE, G., BAZIN, P., PICHON, P., BENGAOUER, A.: CCFL in Hot Legs and Steam Generators and Its Prediction with the CATHARE Code, Proceedings of the 7th Int. Topical Meeting on Nuclear Reactor Thermal Hydraulics, Saratoga Springs, USA, 1995: 815-826.

[35] RICHTER, H. J., WALLIS, G. B., CARTER, K. H., MURPHY, S. L.: Deentrainment and Countercurrent Air-water Flow in a Model PWR Hot-leg, NRC-0193-9, Washington, D. C., US Nuclear Regulatory Commission, 1978.

[36] VALLÈE, C., SEIDEL, T., LUCAS, D., BEYER, M., PRASSER, H.-M., PIETRUSKE, H., SCHÜTZ, P., CARL, H.: Counter-current Flow Limitation Experiments in a Model of the Hot Leg of a Pressurized Water Reactor – Comparison between Low Pressure Air/water Experiments and High Pressure Steam/water Experiments, Proceedings of the 13th Int. Topical Meeting on Nuclear Reactor Thermal Hydraulics, N13P1107, Kanazawa, Japan, 2009.